Performance and outlook for the SADAR array network at the Newell County facility

Paul A. Nyffenegger[1]*, Jian Zhang[1], Elige B. Grant[1], Derek Quigley[1], Kevin D. Hutchenson[1], Mark A. Tinker[1], Don C. Lawton[2,3] and Marie Macquet[2] summarise results from a year of monitoring of the Newell County facility using the SADAR permanent array network, including an updated seismic velocity model determined from ground truth calibration events and quantified estimates of system performance.

Abstract

Since installation in November 2021, a sparse network of SADAR compact volumetric arrays has been continuously and persistently acquiring data for passive microseismic monitoring of the Newell County Facility (NCF) CO_2 storage pilot site. This report summarises several fundamental results from a year of continuous monitoring of the NCF using the SADAR permanent array network, including an updated seismic velocity model determined from ground truth calibration events, the observed seismicity derived from the curated year-long bulletin, and quantified estimates of system performance. In particular, the bulletin includes more than 560 analyst-verified located events excluding those at the surface, with at least 200 considered to be well-located. We have documented noise reduction provided by coherent processing of SADAR array data in excess of 30 dB compared to surface sensors and signal-to-noise ratio (SNR) improvements up to 20 dB compared to single channels. Combining the bulletin information and performance measurements, we estimate magnitude of completeness $M_c \approx -2.5$ Mw, and an event-to-receiver range for locatable events of at least 600 m from individual arrays. We conclude with a look at continuing and planned projects using the SADAR network at the NCF including tests of active source acquisition.

Introduction

For geological carbon storage (GCS) to contribute significantly to the reduction in emissions of greenhouse gases, this technology needs to be upscaled to gigatonne volumes. Monitoring of GCS projects is critically important for verifying both containment and conformance of CO_2 in the storage complex. Continuous passive microseismic monitoring and time-lapse active source seismic surveys are two key monitoring strategies for large-scale GSC projects. Real-time capture and analysis of microseismic events associated with CO_2 injection is paramount for public assurance and containment verification, and the same permanently installed receiver arrays may be used for monitoring conformance using sparse active-source surveys.

The Containment and Monitoring Institute (CaMI) of Carbon Management Canada developed and operates the Newell County Facility (NCF) in Southern Alberta shown in Figure 1, a CO_2 storage pilot site for evaluating measurement, monitoring, and verification (MMV) technologies (Lawton et al. 2019; Macquet et al. 2019). A small and controlled volume of CO_2 is injected into the Basal Belly River Sandstone (BBRS, z=300m) and enables development and testing of MMV tools toward minimising risks associated with GCS (Macquet et al. 2022). A comprehensive suite of MMV tools is deployed at the site: active seismic 2D, 3D, and vertical seismic profile (Kolkman-Quinn et al., 2023), electrical resistivity, distributed acoustic sensing, distributed temperature sensing, and water and gas samplings. For microseismic monitoring specifically, permanent seismic instrumentation (Figure 2) includes a surface network of 28 three-component geophones buried at 1m depth, a downhole array of 24 three-com-
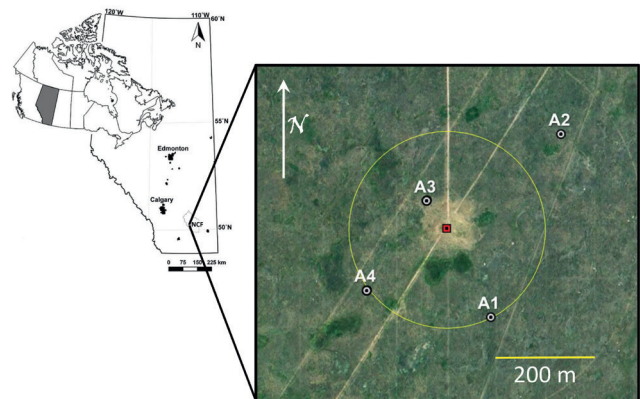

Figure 1 Map showing Newell County Facility location with respect to Alberta, Canada, and a zoomed in view showing the location of the four SADAR arrays A1 through A4 and the injection well (red square, centre) with a 200 m range-ring plotted as the yellow circle (after Macquet et al. 2019, and Hutchenson et al. 2023).

During preparation of this paper, Jian Zhang, one of the authors, died suddenly. All at First Break send our condolences to his family, colleagues and friends.
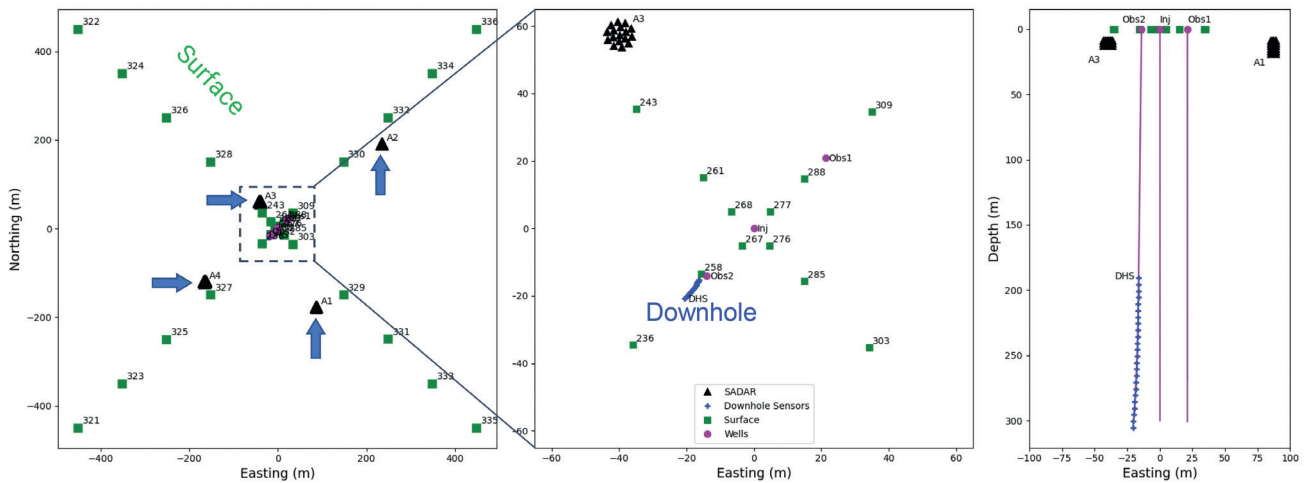
Figure 2 (Left) Map of Newell County Facility showing the four SADAR arrays (blue arrows and triangles) and 3C surface geophones (squares) relative to injection and monitoring wells. (Centre) Zoomed-in view of Newell County Facility emphasising SADAR array A3, the injection well and two observation wells (purple dots) and the downhole array (blue crosses). (Right) Vertical cross-section along an East-West transect showing A1 and A3, the injection well at centre (Inj), the observation wells (Obs1 and Obs2), and the downhole array (DHS) (after Zhang et al. 2023).
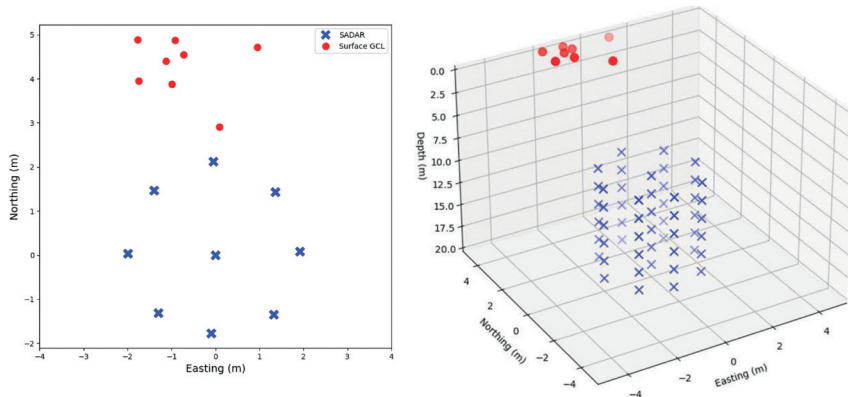

Figure 3 (Left) Map view of array design (1) used for A1 and A2. (Right) Three-dimensional view for A2. A surface cluster of Geospace GCL 3C units was also emplaced above A2 (red circles) (from Nyffenegger et al. 2023).

ponent geophones extending to injection zone depth, and four geophone compact volumetric phased arrays (SADAR arrays) (Macquet et al. 2022, Zhang et al. 2023a).

In November 2021, Quantum Technology Sciences, Inc. (Quantum), in cooperation with the NCF, installed the sparse network of four SADAR arrays, designed specifically to enable real-time monitoring of microseismic activity associated with the CO_2 injection activities (Nyffenegger et al. 2022; Zhang et al. 2022a; Zhang et al. 2023a). In comparison with the receiver groups commonly used in active source seismic surveys, SADAR arrays enable a steerable response pattern and a variety of processing techniques documented in the phased array body of knowledge (Zhang et al. 2023a, Nyffenegger et al. 2023).

The objectives for SADAR array MMV applications are optimising the SNR, determining an unambiguous angle-of-arrival, and measuring the true phase velocity of the arriving signals. The SADAR array's three-dimensional response and ability to apply spatially coherent processing (beamforming) of N elements provides an expected upfront $10 \log N$ dB SNR gain over a single channel for uncorrelated noise (Urick 1983). The SNR gain also reduces the uncertainty in estimated phase arrival times, reducing event location uncertainties. In addition, the beamforming operation suppresses coherent noise arriving at the array from directions other than the beam main response axis (MRA) (e.g. Abraham 2019).

In comparison to surface patch array networks and borehole arrays, permanent SADAR arrays have a reduced surface footprint, reduced infrastructure, reduced cost for emplacement, and more easily serviceable components, while providing both noise reduction and signal enhancement. Scalability, persistent real-time data acquisition and array and network processing for passive monitoring applications is inherent to the system architecture. In addition, the architecture design allows the SADAR network to grow incrementally with the state and understanding of the CO_2 plume or the progression of seismicity while accommodating cultural features.

Nyffenegger et al. (2022) described the NCF SADAR network and provided initial examples of gains. In this report, we review the instrumentation and installation, and provide a summary of results after a year of continuous passive monitoring. Highlights include the development of an improved compressional wave velocity model, a seismicity bulletin, a framework for assessing performance and measurements of noise suppression and detection range. The bottom line is that the arrays are performing as designed and coherent processing is providing the substantial SNR gains that enable low uncertainty location and an estimated magnitude of completeness of $M_c \approx -2.5$ Mw. Lastly, we present an outlook of continuing project activities and goals, including an approach for evalu-
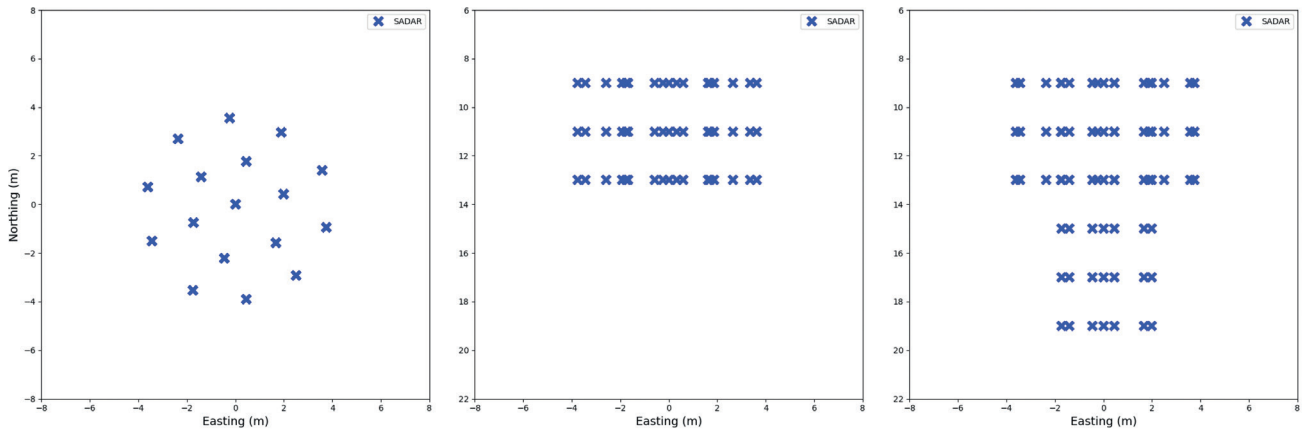
Figure 4 Array designs (2) and (3) used for A3 and A4 respectively. (Left) Map view is identical for both designs. (centre) Cross-section for design (2) which is limited to three levels. (Right) Design (3) cross-section extends the inner hexagon to six levels (after Nyffenegger et al. 2023).

ating effectiveness of sparse active-source seismic surveys for large-scale GSC projects.

Accomplishments

Installation of the four permanent arrays commenced on 11/12/2021. Seven days later, all arrays and acquisition components were complete, and the initial data were flowing into a portable controller unit for logging. The network has been logging data continuously since the November 2021 installation.

Three different variations of nested uniform cylindrical arrays of multiple layers shown in Figure 3 and Figure 4 are used for the four arrays (Zhang et al. 2023a, Nyffenegger et al. 2023). Sensor counts per array range between 51 and 72 vertical-oriented geophones. The array elements are installed in boreholes at depths of 9 m to as deep as 19 m and grouted in place. Geospace GS-ONE 10 Hz geophones occupy all elements and data are acquired at 2000 samples per second using single channel 24-bit digitizers generating ~4.3 terabytes per month (SEG-D format). In addition, for noise comparison purposes, Quantum deployed eight Geospace GCL 3C packages having GS-SMG 10 Hz sensors at array A2 over 05/30/2022-06/20/2022 arranged as a tripartite array and a small aperture receiver group. The network design enables performance assessments of the different array designs given the expected locations of events at the NCF.

Achieving the low uncertainty event locations required for monitoring microseismic events within a geologic reservoir requires a well-resolved velocity model. The preferred method for generating an accurate velocity model depends on ground truth events, manually picking phase arrivals, and optimising the velocity model to minimise differences between the observed and modelled arrival times. Processing that improves the SNR to show clear phase onsets supports this objective.

We use both surface hammer strikes and a deep maintenance event within Observation Well #2 (OBS2) for ground truth events to improve an initial velocity model derived from sonic well logs (Zhang et al. 2023b). The deep event consists of a well-swabbing operation that generated an impulsive source which was successfully detected across the downhole array and the SADAR network, with a moment magnitude Mw=-1.6 determined using the SADAR arrays. The surface hammer events are not detectable on the downhole array, and the deep well-swabbing event was not

detected over the surface network. However, SNR improvements resulting from beamforming allow phase arrival time estimates with uncertainties averaging 2 ms from the SADAR network data.

Including the deep swabbing event location requires increasing the velocities below 150 m by 20% (Figure 5) to minimise the difference between the picked and modelled arrival times. The updated, calibrated velocity model provides a location for the deep event having a 95% coverage ellipse with dimensions [27 m, 16 m, 55 m] for semi-major axis, semi-minor axis and depth respectively, that contains the ground truth location (Figure 6). Nevertheless, we cannot completely resolve an accurate velocity model across all depths for the monitored earth volume using only one deep ground truth event.

An accurate velocity model enables continuous microseismic monitoring in the form of event detection and location which then enables creation of a curated seismicity bulletin for the volume within the network (Hutchenson et al. 2023). The event location procedures used for building the bulletin are discussed in Zhang et al. (2022a) and Zhang et al. (2023a). After a year of monitoring starting in November 2021 through to mid-December
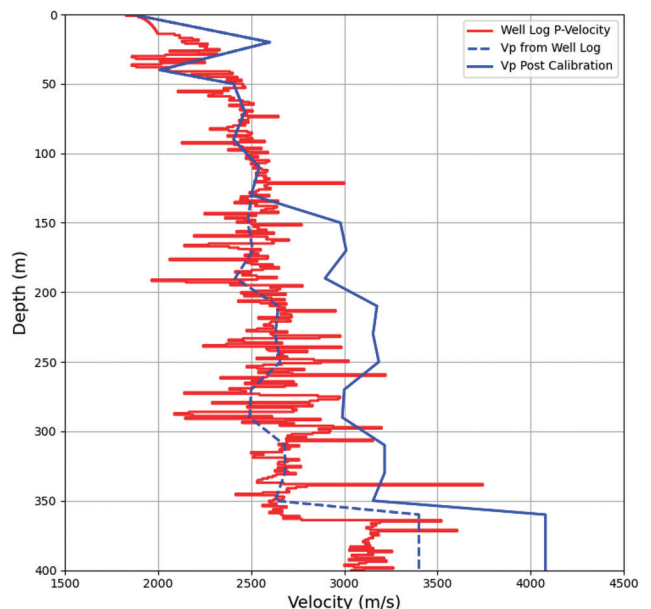

Figure 5 Calibrated velocity model compared with the initial model derived from well logs (after Zhang et al. 2023b).
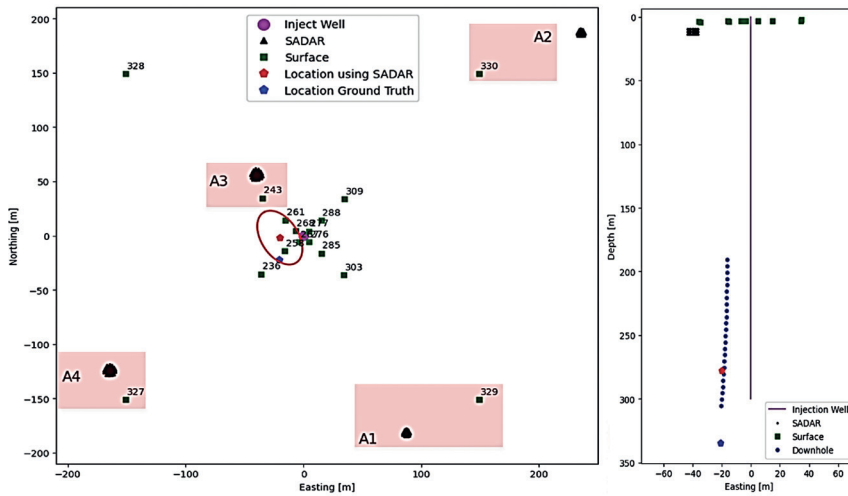
Figure 6 (Left) Map view of the SADAR arrays (black triangles) and the surface network (green squares), and (right) east-west cross section showing the estimated location of the deep-swabbing event (red pentagon) with uncertainty ellipse outline in red, after velocity model calibration, and with the ground truth location (blue pentagon) (from Zhang et al. 2023b).
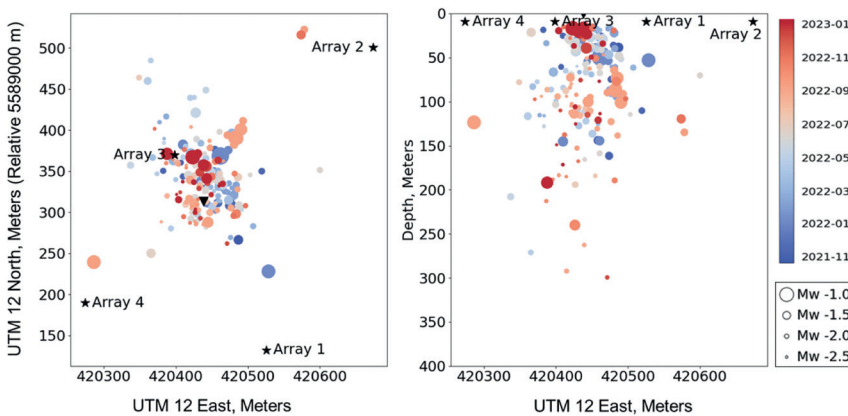

Figure 7 (Left) Map view and (right) east-west cross section of the NCF showing SADAR array locations and epicentre and depth of 200 well located events with z > 15m (from Hutchenson et al. 2023). In the cross-section, the injection wellhead location is shown as the small inverted triangle at zero depth, left of centre.
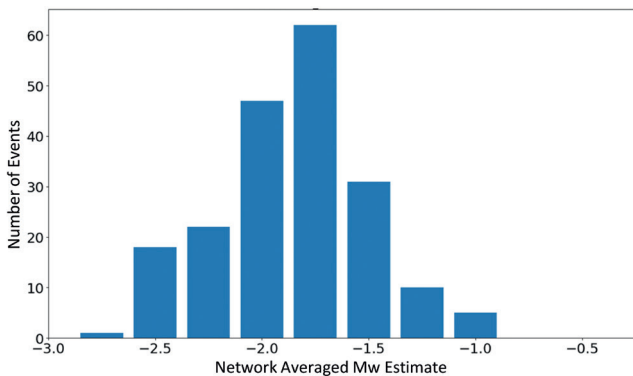

Figure 8 Histogram of network-averaged event moment magnitude Mw for well located events drawn from the SADAR network bulletin for the NCF (from Hutchenson et al. 2023).

2022, the bulletin contains 563 events observed at all four arrays, with lateral location uncertainties as low as 10 m. Removing any suspect events resulting from activities at the surface or at very shallow depths results in approximately 200 well-located events. The majority of these events, shown in Figure 7, locate within 100 m of the injection well. Most events locate with depths above 150 m with a few deeper events, but no significant seismicity is observed within the injection formation.

Having low-uncertainty locations also enables the assessment of event moment magnitude following Brune (1970, 1971). For each event, the magnitude at each station is computed by fitting the displacement spectrum calculated from the optimal beam

with a Brune model between 10 Hz and 90 Hz, then averaged to obtain a network magnitude. The Mw distribution for the group of well-located events is shown in Figure 8; the average observed event magnitude for the entire bulletin is ~Mw -1.75.

The analysis of the bulletin population allows assessment of the performance of the arrays for detection and location as a function of source level and other parameters. Here we focus on detection and provide an assessment of the array gain against noise and the effect of a simple propagation loss. A common mathematical framework for the measurements and performance assessment is developed for passive sonar analysis (e.g. Urick, 1983; Burdic, 1991; Ainslie, 2010; Abraham, 2019). However, the passive sonar framework shares elements with Choy et al. (2001) and Boatwright et al. (2002).

Given $y_i(t,f)$, the suite of received signals from array elements i, let $\Psi()$ represent processing operations such that $\alpha(t,f) = \Psi(y_i(t,f))$ are the processed data. For example, let $\alpha(t,f,\phi,\theta)$ represent a beam having MRA with orientation (ϕ,θ) aligned along the direction of arrival of our particular signal of interest (SOI). Noise and coherent clutter signals not aligned along the beam MRA are suppressed by the series of operations comprising $\Psi()$, but the coherent SOI is largely unmodified. The problem focus becomes identifying the SOI in the presence of competing and interfering unknown signals originating with uninteresting sources, all embedded within a variety of unknown noise. Detecting the SOI requires some measure derived from $\alpha(t,f)$ to surpass a minimum threshold usually related to a required

probability-of-detection. The short-term average (STA) power written $|\alpha(t,f)|$ is a commonly used measure, casting the STA in terms of the expectation of SNR power $\mathbb{S}$ yields,

$$E\left[\mathbb{S}\right] = \frac{\left|\alpha\left(t,f\right)\right|}{E\left[noise\left(\alpha\left(t,f\right)\right)\right]} \geq threshold \qquad . \qquad (1)$$

The expected noise power component (denominator above) must be statistically estimated over several analysis frames and is generally non-stationary. Starting with this equation, casting the expression into decibels (dB), and then following the approaches used for the passive sonar equation results in an equation for signal excess SE, the portion of SNR that is greater than the detection threshold:

$$\mathrm{SE} = \left[\left(SL - RP\right) - PL - \left(NL_f - \left(AG + SP\right)\right) + PG\right] - \mathrm{DT} \quad \mathrm{dB} \quad (2)$$

where SL is the source level; PL is the propagation loss; NL_f is the noise spectrum level; AG is the array gain; and PG is gain due to signal processing after beamforming but within $\Psi()$. Frequency dependence is implicit in each term. The radiation pattern factor RP and sensitivity pattern of the sensor elements SP are neglected here. Nyffenegger et al. (2023) more fully discuss the development of Equation 2.

Ignoring RP and SP, this equation identifies six degrees of freedom for signal detection. In passive microseismic event detection, the noise level NL_f is the limiting factor, and the most effective way to minimise noise levels is to place sensors at depth away from surface noise sources. However, a properly designed phased array enables arbitrary directional beamforming, suppressing uncorrelated noise components as well as coherent signals having a direction of arrival not aligned with the beam MRA and improving the noise measure in comparison to emplacement depth alone. Array gain estimates derived from simple SNR measurements using the optimal beam compared to

array single channel values for several individual events indicate values between ~8 dB and ~20 dB can be expected (Zhang et al. 2022b). However, results for some events, compared with surface sensors, are not as favourable (~4 dB) (Zhang et al. 2023a) indicating that additional processing is required to cancel coherent noise, or that the signal is losing coherence over the aperture of the array as it propagates from the hypocentre.

Figure 9 summarises results comparing the noise levels of SADAR arrays against the other seismic instruments at the NCF. As expected, the temporary GCLs and permanent NCF surface sensors record elevated noise spectral levels compared to the SADAR arrays. The downhole sensor measurements (in blue, Figure 9 left graph) appear to have an elevated noise floor compared to the other systems; we expect that this is the result of non-optimal recording settings, and we exclude these sensors from further analysis.

For the SADAR arrays and permanent geophones, Figure 9 indicates ambient noise levels in the band 0 Hz - ~70 Hz that fall off with frequency, transitioning to a steady-state noise floor above 100Hz typical of sensor and acquisition system self-noise processes. Spectra for the GCL cluster transitions to approximate steady-state noise levels above ~400 Hz (not shown). The suppression of noise levels provided by increasing emplacement depth alone for the band 30Hz-100Hz is between ~15 dB - 25 dB comparing the GCL sensors vertical channel and A2 single channels, and averages ~19 dB for the NCF geophones at 1m depth. For f > 100 Hz the GCL-A2 single channel difference spans ~8 dB - 16 dB, and the NCF-A2 single channel difference averages ~13 dB.

For estimating array gain, the channels for each array were stacked as an incoherent sum to approximate a beam (Figure 9 black dotted line). In the band 40 Hz - 100 Hz for the spectra of the stack vs. single channel average noise, for A2 the gain spans 8dB - 17dB and for A3 the gain averages ~16 dB. In this same band, the difference in the noise measured from the stack for the SADAR arrays compared to the near-surface geophones
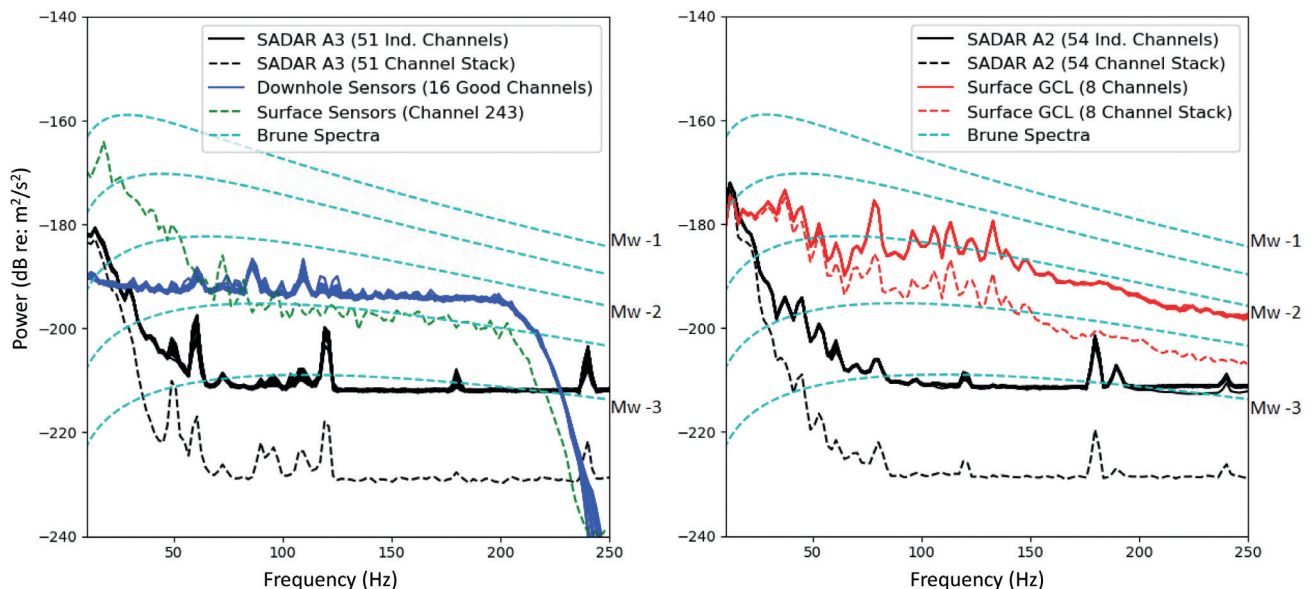

Figure 9 Power spectra for 0.5 s time frames and 10 s records, and theoretical event spectra (Brune 1970, 1971). (Left) Noise levels for seismic instruments proximate to A3, closest to the Injection well. (Right) Noise levels for instruments proximate to A2. Brune spectra computed assuming [Vp,Vs] = (2500m/s, 1100m/s), density =2400kg/m³, Q = 50, Stress Drop = 10kPa, and at a source-receiver range of 300 m.
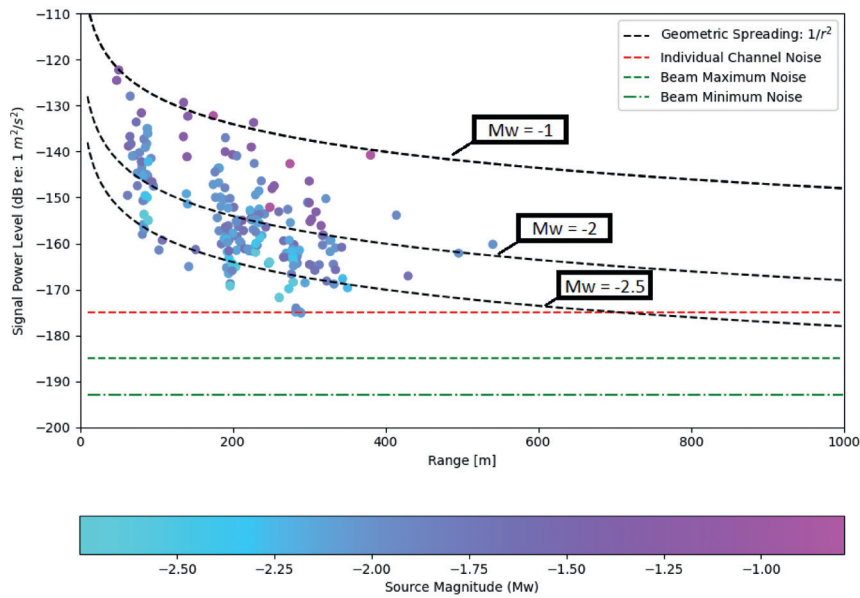
Figure 10 Scatter plot of received signal power vs. source-receiver range for 50 reviewed, well-located events colour-coded relative to event moment magnitude Mw. Black dashed lines are modelled received signal levels for Mw=[-2.5, -2, -1] assuming only spherical spreading propagation loss. The low-noise estimate in the 30-90 Hz band averaged over all array single channels is superimposed (red-dashed line), and the calculated levels after applying the measured gains of ~10 dB (green-dashed line) and ~18 dB (dot-dash line) are plotted below (from Nyffenegger et al. 2023).

averages ~36 dB for A2 and ~34 dB for A3. These gain estimates over the single channel surface emplacements are attributable to both deploying the arrays at depth and the coherent processing array gain. For the steady state region above 100 Hz, noise levels from the stack are suppressed by ~17 dB compared to the SADAR array single channels which agrees with the theoretical $10 \log N$ dB figure (Urick, 1983).

Figure 9 also illustrates theoretical Brune (1970, 1971) spectra for five different-sized microseismic events from Mw -3 up to Mw -1 for a source-receiver range of 300 m. Even under ideal noise levels surface sensors would struggle to detect let alone locate events smaller than Mw ~-2 without the gains from processing large and dense networks. However, using the optimal beamformed trace should allow the network of SADAR arrays to automatically detect, identify phase arrival times and perform a location, for Mw -2.5 events occurring throughout the monitored volume.

Referring to Equation (2), the propagation loss *(PL)* factor acts against source level *(SL)*. Propagation loss is a compound factor that includes geometric spreading, attenuation, and backscatter losses at interfaces (Nyffenegger et al. 2023). Detection performance versus range is also proportional to *PL* which can be estimated using the event magnitude and peak signal values recorded in the seismicity bulletin. For 50 events having low location uncertainty, Figure 10 graphs the peak received signal power measured from the optimal beam for each array as a function of the event magnitude (i.e. source level) versus event-to-array range. The average array single-channel low noise estimate (red-dashed line) and the low noise estimates associated with measured gains of ~10 dB minimum to ~18 dB maximum (green dash and dash-dot lines, respectively) are superimposed on the measured received signal level plot. Assuming reliable detection and location requires a signal excess SE>= 10 dB, and considering the superimposed geometrical spreading represents a maximum expected signal level, the integrated information suggests that detection and location of ~Mw = -2.5 events is limited to a maximum range between 600 and 800 m from any array. Furthermore, the upper dashed-green line in Figure 10 also suggests that the threshold for event detection at any individual SADAR array is below Mw = -2.5 at ranges out to 800 m, which which roughly agrees with estimates of event detectability for the Brune models shown in Figure 9.

Outlook

The sparse network of SADAR compact volumetric arrays at the NCF has operated persistently and reliably over the past year, yielding a seismicity bulletin population of 563 events and growing, but more importantly providing a seismicity baseline prior to any geomechanical changes originating from injections of large volumes of CO_2. The four SADAR arrays comprise a total of 231 channels yet occupy only ~150 m² total on the surface. In terms of noise suppression and SNR improvement metrics, the observed performance heavily favours coherently processed SADAR arrays. In terms of continuous microseismicity monitoring, the SADAR network and processing system reliably locates microseismicity at least down to Mw ≈ -2.5 at source-receiver ranges that analysis indicates extend 600 m - 800 m.

Quantum plans to continue passive microseismic monitoring at NCF and building out the bulletin. Certainly, a priority moving forward is the migration of NCF monitoring to near real-time processing. Implementing the existing processing pipeline for automatically generating the bulletin wholly unsupervised within the current scalable system architecture is the ultimate goal. As engineering and operational activities modify the NCF reservoir, any emerging seismicity patterns will be documented at least down to Mw ≈ -2.5. We are also working towards more completely quantifying the individual factors identified in the performance model, especially a more detailed understanding of noise levels aimed towards coherent noise suppression and propagation loss to include attenuation and back-scatter factors. Quantifying the model factors allows the assessment and prediction of the network performance for detection, location, and M_c as a function of depth and lateral location within the monitored volume. Fusing the information in the bulletin with the quantified performance will allow for a better geomechanical understanding by matching Q and stress drop to better estimate Mw.

For upscaling carbon capture and GCS projects, innovative seismic MMV approaches will be required to constrain costs. At gigatonne-scale storage, conventional time-lapse 3D seismic surveys for tracking the CO_2 plume will become prohibitively expensive as the plume volume increases. One proposed monitoring approach (Lawton et al. 2022) is to use sparse networks of permanent seismic sources and receivers deployable on an expanding basis with GCS project growth. SADAR arrays used as receivers in these active source seismic surveys will be economical and potentially the most effective instrumentation, with appropriate surveys designed to maximise the SNR of key targeted reflections. These sparse, time-lapse active surveys would image the arrival of the plume at key locations without impacting the continuous, real-time passive microseismic monitoring functions. Over the next 12 months Carbon Management Canada will be installing a permanent source at the NCF and testing active source recording into the SADAR arrays at the site.

Acknowledgements

References

Abraham, D.A. [2019]. *Underwater Acoustic Signal Processing*, Springer Nature Switzerland, Cham.

Ainslie, M.A. [2010]. *Principles of Sonar Performance Modeling*, Springer-Verlag Berlin.

Boatwright, J., Choy, G.L. and Seekins, L.C. [2002]. Regional estimates of radiated seismic energy. *Bulletin of the Seismological Society of Americ,* **92**, 1241-1255.

Brune, J. [1970]. Tectonic stress and the spectra of seismic shear waves from earthquakes, *Journal of Geophysical Research*, **75**, 4997-5009.

Brune, J. [1971]. Correction, *Journal of Geophysical Research*, **76**, 5002.

Burdic, W.S. [1991]. *Underwater Acoustics System Analysis, Second Edition*, Prentice-Hall, Englewood Cliffs.

Choy, G.L., Boatwright, J.L. and Kirby, S. [2001]. The radiated seismic energy and apparent stress of interplate and intraplate earthquakes at subduction zone environments: implications for seismic hazard estimation, *USGS Open File Report 01-0005,* U.S. Geological Survey.

Hutchenson, K.D., Quigley, D., Zhang, J., Grant, E.B., Nyffenegger, P.A., Jennings, J., Tinker, M., Dahl, M., Grindell, D., Lawton, D.C. and Macquet, M. [2023]. Microseismic monitoring using SADAR arrays at the Newell County carbon storage facility: what have we learned in a year?, Extended abstract accepted to Geoconvention 2023.

Kolkman-Quinn, B., Lawton D. and Macquet, M. [2023]. CO2 leak detection threshold using vertical seismic profiles, *International Journal of Greenhouse Gas Control*, **123**, 103839.

Lawton, D.C., Dongas, J., Osadetz, K., Saeedfar, A. and Macquet, M. [2019]. Chapter 16: Development and analysis of a geostatic model for shallow CO2 injection at the Field Research Station, Southern Alberta, Canada, in: Davis, T., Landro, M., and Wilson, M. (Eds), *Geophysics and Geosequestration.* Cambridge University Press, 280-296. DOI 10.1017/9781316480724.017.

Lawton, D., Hinter, T., Kolkman-Quinn, B., Monsegny, J., Bertram, M. and Maidment, G. [2022]. Sparse Optimum-offset, Seismic Surveys for Monitoring Gigatonne-scale CCS Projects. SEG Summer Research Wokshop: *Toward Gigatonnes CO2 Storage — Grand Geophysical Challenge*; 26-30 June 2022, Stanford, CA.

Macquet, M., Lawton, D.C., Saeedfar, A. and Osadetz, K. G. [2019]. A feasibility study for detection thresholds of CO2 at shallow depths at the CaMI Field Research Station, Newell County, Alberta, Canada, *Petroleum Geoscience*, **25**(4), 509-518.

Macquet, M., Lawton, D.C., Osadetz, K., Maidment, G., Bertram, M., Hall, K., Kolkman-Quinn, B., Monsegny Parra, J., Race, F., Savard, G. and Wang, Y. [2022]. Overview of Carbon Management Canada's pilot-scale CO2 injection site for developing and testing monitoring technologies for carbon capture and storage, and methane detection, *Recorder*, **47**, 1-27.

Nyffenegger, P.A., Tinker, M.A., Zhang, J., Grant, E.B., Hutchenson, K.D. and Lawton, D.C. [2022]. Compact phase arrays for microseismic monitoring, *First Break*, **40**(4), 69-74.

Nyffenegger, P.A., Grant, E.B., Zhang, J., Jennings, J., Quigley, D., Hutchenson, K.D., Tinker, M., Macquet, M., Lawton, D.C. [2023]. *Estimates of performance model factors for passive microseismic SADAR phased arrays at the Newell County Facility*, Extended abstract accepted to Geoconvention 2023.

Urick, R.J. [1983]. *Principles of Underwater Sound, 3rd Edition*, Peninsula Publishing, Westport.

Zhang, J., Grant, E.B., Nyffenegger, P., Tinker, M.A., Hutchenson, K.D. and Lawton, D.C. [2022]. Seismic monitoring using compact phased arrays: CO2 sequestration monitoring. *Second International Meeting for Applied Geoscience & Energy. August 2022*, Extended Abstracts, 483-487.

Zhang, J., Hutchenson, K.D., Nyffenegger, P.A., Grant, E.B., Jennings, J., Tinker, M., Macquet, M. and Lawton, D.C. [2023a]. Performance comparison of compact phased arrays and traditional seismic networks for microseismic monitoring at a CO2 sequestration test site, *The Leading Edge,* **42***,* in press.

Zhang, J., Nyffenegger, P.A., Hutchenson, K.D., Grant, E.B., Jennings, J., Quigley, D., Tinker, M., Dahl, M., Grindell, D., Macquet, M. and Lawton, D.C. [2023b]. *Velocity calibration for microseismic monitoring at the Newell County carbon storage facility using SADAR compact phased arrays*, Extended abstract accepted to Geoconvention 2023.

Zhang, J., Tinker, M., Hutchenson, K.D., Grant, E.B. and Nyffenegger, P.A [2022]. Seismic monitoring at a CO2 storage site using compact phased arrays, presented at the SEG workshop: *Toward Gigatonnes CO2 Storage — Grand Geophysical Challenge*; 26-30 June 2022, Stanford, CA.